AIAA JOURNAL
Vol. 48, No. 3, March 2010

Numerical Simulation of Glass-Fiber-Reinforced Aluminum Laminates with Diverse Impact Damage

Hyoungseock Seo,* Jake Hundley,* H. T. Hahn,† and Jeen-Ming Yang‡
University of California at Los Angeles, Los Angeles, California 90095

DOI: 10.2514/1.45551

This paper presents a finite element model used to simulate the impact response of a fiber metal laminate. The load-time history, maximum deflection, and damage progression caused by impact loading were examined using an explicit finite element model. Two- and three-dimensional failure criteria in the commercial finite element code ABAQUS are used to model stiffness degradation in the glass-fiber-reinforced composite layers of the laminates. The finite element results showed good agreement with experimental measurements.

Nomenclature

$\boldsymbol{C}_{ij}$	=	material stiffness matrix
C_{ijkl}	=	material stiffness tensor
d	=	material degradation factor
E_{11}	=	composite modulus along the fiber axis
E_{22}	=	composite modulus transverse to the fiber axis
F_i	=	body force vector
f^{fc}	=	Hashin fiber compression failure initiation
f^{ft}	=	Hashin fiber tension failure initiation
f^{mc}	=	Hashin matrix compression failure initiation
f^{mt}	=	Hashin matrix tension failure initiation
G_{12}	=	shear modulus fiber–matrix direction
I_{ijkl}	=	fourth-order identity tensor
$\boldsymbol{S}_{ij}$	=	material compliance matrix
S_{ijkl}	=	material compliance tensor
T_i	=	surface traction vector
t	=	time value at the current finite element analysis increment
U	=	internal energy per unit volume
v_i	=	velocity vector
W	=	internal energy
w^i	=	damage-state variable for each failure mode i
$\dot{w}^i$	=	damage propagation rate for each failure mode i
Δt	=	time step between successive increments
ε_{ij}	=	material strain state
$\dot{\varepsilon}_{ij}$	=	strain rate
$\varepsilon_{ij+}^{\mathrm{init}}$	=	tensile strain component at failure
$\varepsilon_{ij-}^{\mathrm{init}}$	=	compressive strain component at failure
σ_{ij}	=	material stress state
υ_{12}	=	Poisson's ratio for the fiber–matrix direction
υ_{23}	=	Poisson's ratio for the matrix–matrix direction
Ω_0	=	damage nucleation-rate constant
Ω_1	=	damage growth-rate constant

I. Introduction

FIBER metal laminates (FMLs) are a family of hybrid metal and composite laminates for aircraft structural applications. Examples of commercially available FMLs include Aramid-reinforced aluminum laminates and GLARE (S2 glass-fiber-reinforced aluminum laminates), which are composed of alternating layers of unidirectional or bidirectional fiber-reinforced prepreg with aluminum alloy sheets. These hybrid laminates combine the beneficial properties of monolithic metals and fiber-reinforced composites, providing superior mechanical properties compared with conventional polymer matrix composites or aluminum alloys [1,2]. Because of their excellent specific mechanical properties for fatigue and impact behavior, FMLs have been applied in aircraft structures as a replacement of high-strength aluminum alloys. Current applications of FMLs include fuselage structures, aircraft leading edges, and other components for which weight reduction and improved damage tolerance are critical [3].

For FMLs, Laliberte and Poon [4] developed a finite element model for GLARE 3-2/1 using the explicit finite element code LS-DYNA. This study used a user-defined material subroutine (UMAT) based on a continuum damage mechanics (CDM) model to incorporate damage growth and initiation in the composite layers. Three different configurations were studied. The first case combined elastic–plastic aluminum layers, elastic composite layers, and a tied interface of composite layers and metal layers. In the second case, the aluminum layers were modeled as elastic–plastic with elastic composite layers and a tie-break interface. The final configuration used elastic–plastic aluminum layer, CDM modeled composite layers, and a tie-break interface. Laliberte and Poon investigated the differences between predicted and measured peak impact force, absorbed energy, and permanent impactor dent depth in each case. The numerical model incorporating the UMAT subroutine and a tie-break interface showed better experimental correlation compared with the numerical models.

For composite materials, previous research has been focused on the development of efficient numerical models for predicting impact damage in the laminates. Prediction of the internal damage provides detailed and comprehensive information on the stress state and delamination induced by low-velocity impact. Li et al. [5] developed an integrated and elaborate numerical model to predict the various internal-damage modes that occur as a consequence of impact. Davies et al. [6] studied barely visible impact damage in glass/polyester and Kevlar/epoxy composite plates. In their paper, numerical modeling of the impact response, including impact force and strain histories, was performed using a proprietary department code, named FE77. Zhang [7] suggested a strategy for predicting and simulating internal damage in carbon/epoxy composite structures by impact behavior. His finite element model of carbon-fiber-reinforced polymer was developed on the nonlinear behavior with deformation, interlaminar delamination, and in-plane fiber and matrix failure. Through his simulation he tried to calculate the impact force history, deflection of impact point, and predict delamination.

Although the impact behavior of FMLs and composite laminates has been studied by several researchers [4–7], the ability of these

Received 19 May 2009; revision received 12 October 2009; accepted for publication 2 November 2009.

*Ph.D. Researcher, Mechanical and Aerospace Engineering Department, Multifunctional Composite Laboratory, 420 Westwood Plaza.

†Professor, Mechanical and Aerospace Engineering Department, Multifunctional Composite Laboratory, and Material Science Engineering Department, 420 Westwood Plaza, Senior Member AIAA.

‡Professor, Material Science Engineering Department.

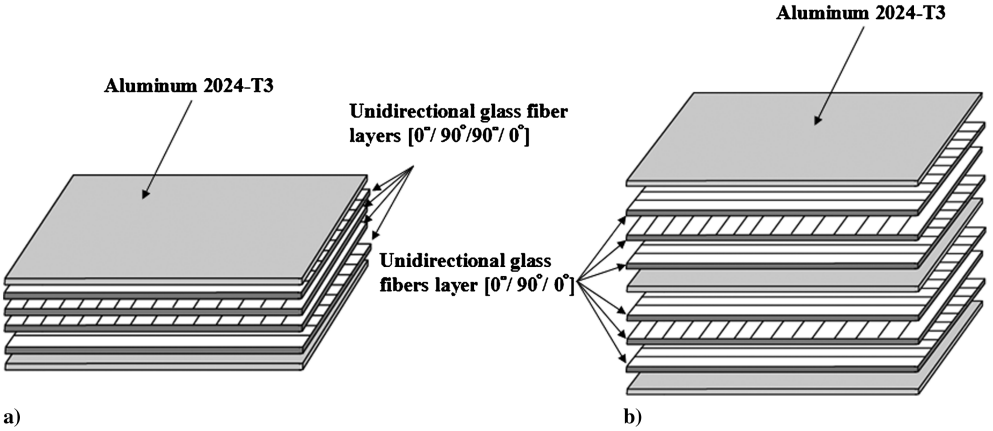

Fig. 1 Configuration of GLARE laminates: a) GLARE 5-2/1 and b) GLARE 4-3/2.

simulations to predict peak impact force, residual stresses, and the internal-damage state is still very limited, particularly for FMLs such as GLARE. Therefore, more finite element studies are needed to accurately predict the dynamic response of GLARE laminates under impact loading.

In this study, finite element simulations were performed to understand and predict the impact behavior of GLARE laminates. Experimental impact results of Wu [1] for two different GLARE variants, GLARE 5-2/1 and GLARE 4-3/2, were used to validate the simulation predictions in terms of peak impact force, deflection, and the internal-damage area. GLARE 5-2/1 consists of two layers of 2024-T3 aluminum alloy and one layer of [0°/90°/90°/0°] glass/epoxy composite, as shown in Fig. 1a. GLARE 4-3/2 is composed of three layers of 2024-T3 aluminum alloy and two layers of [0°/90°/0°] glass/epoxy composite, illustrated in Fig. 1b. For each GLARE variant, the commercial finite element software ABAQUS [8] was used to simulate impact behavior and a three-dimensional explicit vectorized user-defined material subroutine (VUMAT) was developed to model fiber–matrix failure in the composite layers based on the Hashin failure criteria. The simulation results were compared with the experimental impact data to validate the finite element model. Additionally, the three-dimensional failure model was compared with a two-dimensional failure model built in to ABAQUS by investigating the damage progression in the composite layers.

II. Finite Element Simulation of the Impact Behavior of GLARE Laminates

A. Impact Test

Wu [1] used a Dynatup model 8250 drop-weight impact tower for low-velocity impact test with impact velocities up to 13.4 m/s. Using a PC-based data acquisition system GRC 930-I with a photodiode velocity detector, experimental data during impact were recorded automatically. After just dropping the impactor, the pneumatic rebound breaks were operated to push up and hold the impactor assembly to prevent multiple impacts. Diverse impact energies were obtained by adjusting the dropping height in low-velocity impact tests. For impact, the specimen was clamped between two steel plates with a 114.3 × 114.3 mm square. They had a circular opening with 31.7 mm diameter at the center. A steel rod of 12.7 mm in diameter with a semispherical end was used with a mass of 6.29 kg as an impactor. Diverse impact energies were applied on the GLARE laminate to create barely visible impact damage (BVID) and clearly visible impact damage (CVID).

B. General Development of Finite Element Modeling of GLARE Laminates

In the finite element model, four different impact energies were studied, corresponding to BVIDs of 11.4 and 12.7 J and to CVIDs of 16.3 and 16.8 J. In the finite element (FE) simulations for GLARE 4-3/2, the average thickness of the aluminum layers was 0.304 mm, with the [0°/90°/0°] composite layers each having a total thickness of 0.458 mm. For the numerical modeling of GLARE 5-2/1, the layer thickness was set at 0.489 mm for the aluminum layers and at 0.584 mm for the [0°/90°/90°/0°] composite layers. Thus, the total laminate thicknesses were 1.828 and 1.562 mm, respectively, for GLARE 4-3/2 and GLARE 5-2/1. Numerical geometry and applied impact energy in numerical simulation are the same as those in the experimental simulations.

To predict the damage caused by impact, the ABAQUS/Explicit solver was used for numerical simulation of each GLARE variant. Before starting the simulation, it is important to select the correct element for this particular application. The ABAQUS/Explicit element library includes two- and three-dimensional modified second-order interpolation elements, including tetrahedral, triangular prism, and hexahedral (brick) elements [9]. In this study, hexahedral solid elements (C3D8R in ABAQUS) were used for the aluminum layers, and the composite layers were modeled with either hexahedral solid elements or hexahedral shell continuum elements (SC8R in ABAQUS). The choice between solid and shell elements for the composite layers depended upon the nature of the failure criteria and the applicability of a plane-stress assumption, as discussed in the following section. Conversely, for the aluminum layers, the stress state within the metal reinforcement should never be approximated using a plane-stress assumption, due to interactions with the adjacent fiber-reinforced epoxy layers [10–12]. The material behavior of aluminum layers was assumed to be isotropic elastic–plastic. The glass-fiber-reinforced composite layers were modeled with a user material subroutine that implemented the full Hashin three-dimensional failure criteria [13] to predict damage initiation and evaluate the damaged material's constitutive response. As will be discussed in the following section, a failure model that incorporates all stress tensor components (i.e., no plane-stress assumption) is necessary in impact simulations, due to the applied loads and boundary conditions present in the model. Additionally, realistic modeling of the interface between the metal- and fiber-reinforced polymer layers requires inclusion of all through-thickness stresses [10–12]. To compare the effects of neglecting all three-dimensional stress tensor components, impact simulation results for GLARE with user-defined solid-element constitutive behavior were compared with results obtained using a built-in planar failure constitutive model for continuum shell elements.

In a dynamic impact simulation, because of excessive distortion of elements it is also important to consider hourglass control for deformable elements [9]. When these elements experience much distortion as a result of impact, zero-energy hourglass modes can be a critical problem for reduced-integration elements such as C3D8R and SC8R in stress/displacement analyses.

Figures 2a–2d show the mesh geometry and boundary conditions for impact simulation of GLARE 5-2/1 and GLARE 4-3/2. As shown in Fig. 2a, the GLARE laminate mesh was modeled based on the size of the impact fixture hole. Figures 2b and 2c show the mesh geometry of GLARE 5-2/1 and GLARE 4-3/2, respectively. For each GLARE variant, only one-half of the laminate's in-plane geometry was

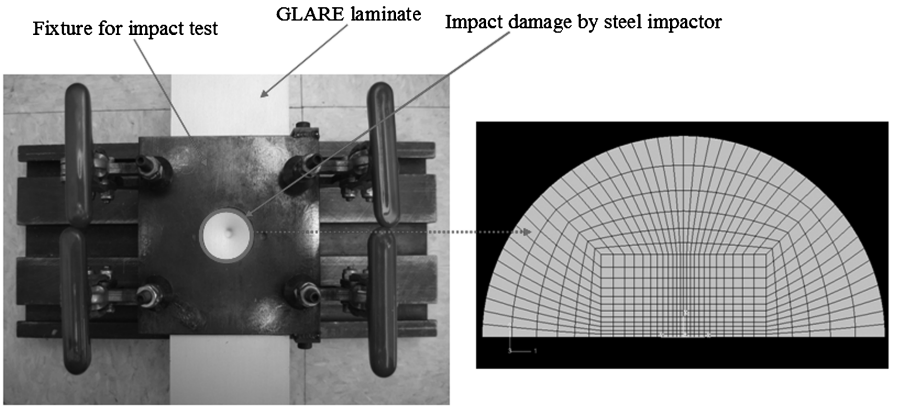

a) Development of finite element model geometry from experimental setup

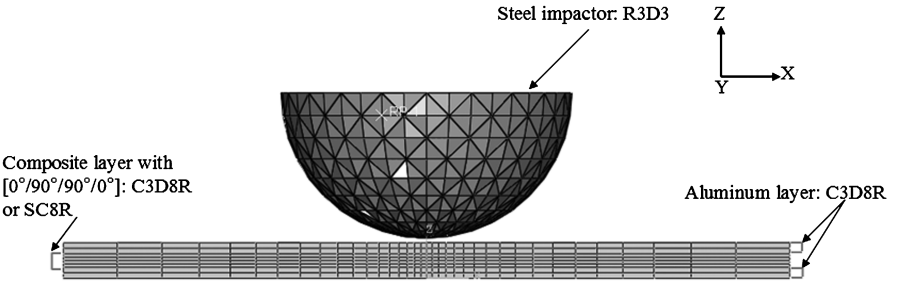

b) Mesh geometry for GLARE 5-2/1

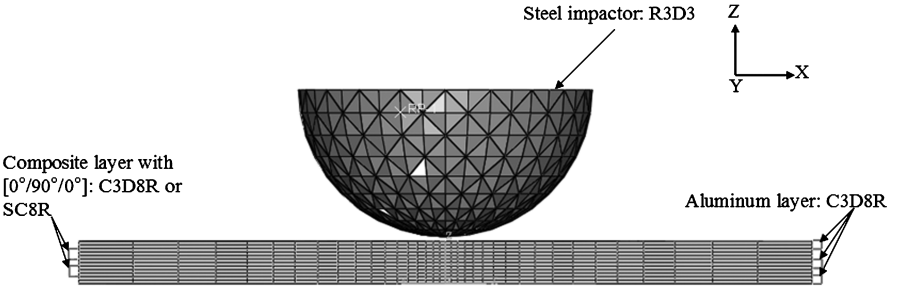

c) Mesh geometry for GLARE 4-3/2

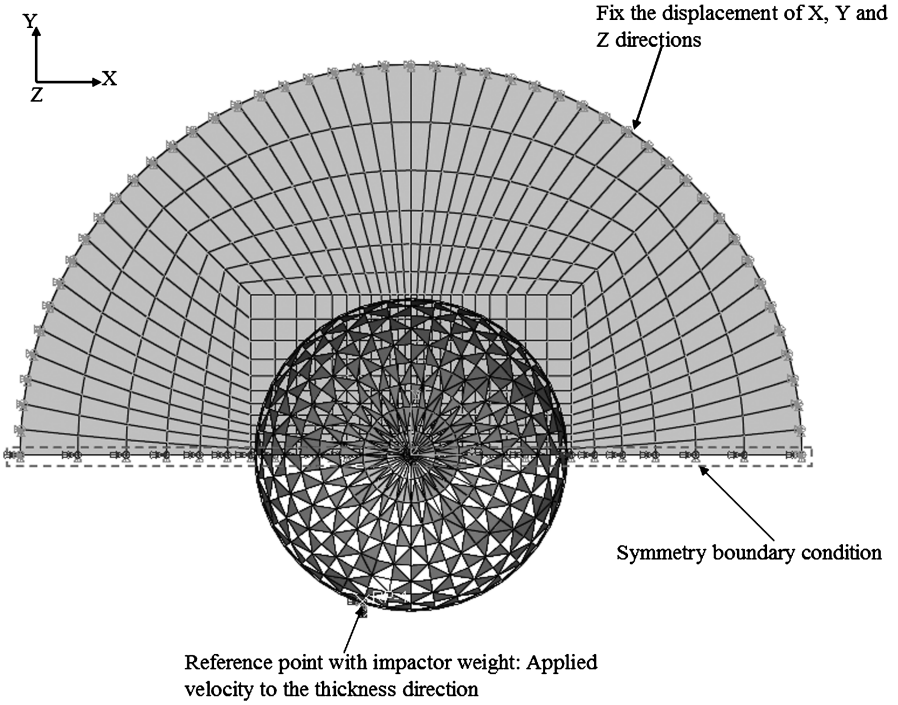

d) Boundary condition of finite element model geometry

Fig. 2 Finite element model geometry and boundary conditions.

modeled with appropriate symmetry boundary conditions applied, as shown in Fig. 2d. At the nonsymmetric laminate boundary, all displacement degrees of freedom were fixed, corresponding to a perfect-clamping assumption. Additionally, the impactor was constrained against motion in the x and y directions, or rotation about the same axes. Because the impactor was made of steel, with a much larger stiffness compared with the GLARE laminate, the impactor was modeled as a perfectly rigid body.

Linear elastic material properties, as well as damage and failure properties [10–12] of aluminum 2024-T3 and S2 glass-fiber-reinforced composite laminate used in the FE simulation are summarized in Tables 1 and 2, respectively.

C. Three-Dimensional Composite Constitutive Modeling

1. *Three-Dimensional Modeling Rationale*

As discussed previously, in typical finite element analyses of composite structures, continuum shell elements (e.g., SC8R) are used to model the composite laminate. Continuum shells combine the planar nature of traditional shells with the three-dimensional geometry of solid elements. As such, they offer a computationally efficient method for simulating systems that are globally three-dimensional but locally planar [14]. A multilayered laminated composite structure is a good example of such a system. Because the mechanical properties of the composite laminate will, in general, vary between subsequent layers, the structure cannot be modeled with a single set of three-dimensional solid elements; each layer must be represented by a unique element set. One layer of a unidirectional tape-based (i.e., not woven) composite typically has a thickness on the order of hundreds of microns, whereas the structure into which it is incorporated has a geometry on the order of meters. Because of this large aspect ratio with respect to the laminate thickness, each layer can be assumed to be in a state of plane stress, with all through-thickness normal and shear components of the stress tensor $(\sigma_{13}, \sigma_{23}, \sigma_{33})$ assumed to be negligible in comparison with their in-plane counterparts $(\sigma_{11}, \sigma_{22}, \sigma_{12})$. Therefore, such a system is technically three-dimensional, but approximately planar, and can be modeled with continuum shell elements.

This planar assumption is valid for most composite structures, but breaks down in several specific instances. The most obvious breakdown scenario is for a thick composite in the limiting case for which the aspect ratio of the laminate width and/or length with respect to the thickness approaches unity. For this system, the laminate thickness is no longer negligible in comparison with the other dimensions, and interlaminar through-thickness stress tensor components must be considered. A second, and perhaps less obvious, scenario that prevents use of continuum shell elements involves the nature of the boundary conditions present in the finite element model. If the boundary conditions are applied such that nontrivial out-of-plane stresses arise in response to their application, then the system is no longer planar and continuum shells should not be used. Such is the case for the finite element model under consideration in the present study (Fig. 3): a rigid impactor incident upon the laminate in a direction aligned with the plane of material isotropy. In this configuration, the direction of impact is parallel to the shell element normal vector (Fig. 3) and therefore will produce nontrivial through-thickness stresses. The plane-stress assumption associated with continuum shell elements is inappropriate in this instance, since it is in direct contradiction with the applied boundary conditions. Another important factor that precludes the usage of continuum shells in an impact simulation is the formation and propagation of delamination zones between the composite laminate. Since delamination is governed by the out-of-plane stress states in consecutive layers, incorporation of all stress tensor components is essential for accurate representation of postimpact delamination.

Table 1 Material properties used in the finite element model [10–12]

Material	Parameter values, GPa					
	E_{11}	E_{22}	G_{12}	G_{23}	ν_{12}	ν_{23}
Al 2024-T3	72.2	72.2	——	——	0.33	0.33
S2 glass	55	9.5	5.5	3	0.33	0.33

Table 2 Damage and failure properties used in the finite element model [10–12]

Material	Parameter value, MPa					
	σ_{ys}	Xt	Xc	Yt	Yc	Slt[a]
Al 2024-T3	320	——	——	——	——	——
S2 glass	——	2500	2000	50	150	75

[a]*Slt* denotes the in-plane shear failure stress.

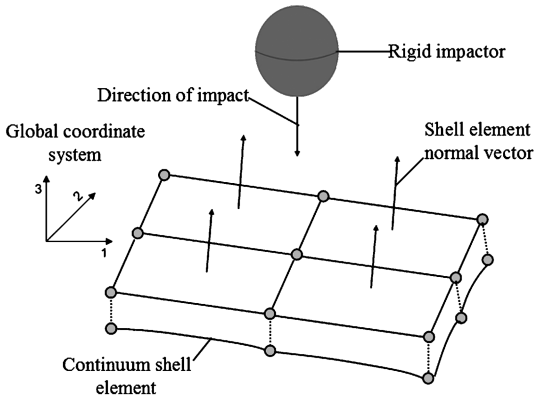

Fig. 3 Continuum shell element normal vector relation to direction of impact.

2. *Three-Dimensional Progressive-Damage Model for Composite Materials*

Because use of planar elements is the norm for finite element analyses of composite materials, progressive damage and failure methodology built in to commercial finite element programs such as ABAQUS necessitate the use of continuum shell elements [9]. As discussed previously, since shell elements are not appropriate for the impact simulation under consideration in the present study, a VUMAT was developed to simulate progressive damage and failure of composite materials with three-dimensional solid elements. The methodology described herein applies to the ABAQUS/Explicit processor but can be adapted to any explicit displacement-based finite element code. For each integration point in the model, the initiation of composite damage is defined using the well-known Hashin failure criteria, expressed in terms of the strain tensor ε_{ij} and experimentally measured strain at failure $\varepsilon_{\mathrm{ij}}^{\mathrm{init}}$ in Eqs. (1–4) [13]. These failure strain values can be obtained from the more widely used failure stress measurements by taking the inner product with respect to the corresponding components of the material compliance tensor. The Hashin criteria allows for four modes of composite damage, illustrated schematically in Fig. 4, with each mode represented by its own normalized failure variable f^i.

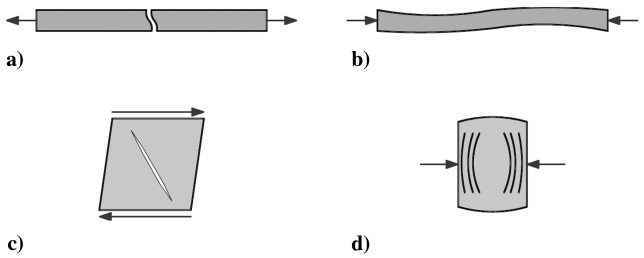

Fig. 4 Hashin composite-failure modes a) fiber tension mode, b) fiber compression mode, c) matrix tension/shear mode, and d) matrix compression mode.

Table 3 Degradation scheme for composite progressive damage

	Degraded elastic material properties				
Failure mode	E_{11}	E_{22}	v_{12}	v_{23}	G_{12}
ft	×	——	×	——	×
fc	×	——	×	——	×
mt	——	×	×	×	×
mc	——	×	×	×	×

Fiber tension (ft) failure mode ($\varepsilon_{11} > 0$):

$$f^{\text{ft}} = \left(\frac{\varepsilon_{11}}{\varepsilon_{11+}^{\text{init}}}\right)^2 + \frac{1}{\varepsilon_{12}^{\text{init2}}}(\varepsilon_{12}^2 + \varepsilon_{13}^2) \geq 1 \tag{1}$$

Fiber compression (fc) failure mode ($\varepsilon_{11} < 0$):

$$f^{\text{fc}} = \frac{-\varepsilon_{11}}{\varepsilon_{11-}^{\text{init}}} \geq 1 \tag{2}$$

Matrix tension/shear (mt) failure mode ($\varepsilon_{22} + \varepsilon_{33} > 0$):

$$f^{\text{mt}} = \frac{1}{\varepsilon_{22+}^{\text{init2}}}(\varepsilon_{22} + \varepsilon_{33})^2 + \frac{1}{\varepsilon_{12}^{\text{init2}}}(\varepsilon_{23}^2 + \varepsilon_{12}^2 + \varepsilon_{13}^2 - \varepsilon_{22}\varepsilon_{33}) \geq 1 \tag{3}$$

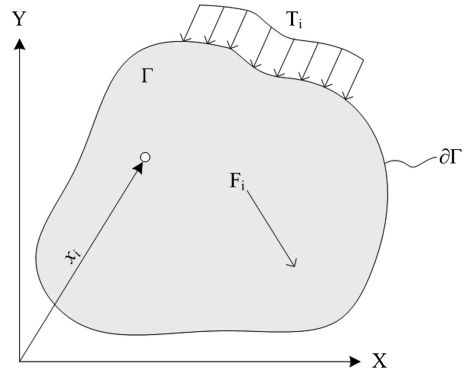

Fig. 5 General schematic for energy dissipation of a continuum body.

Matrix compression (mc) failure mode ($\varepsilon_{22} + \varepsilon_{33} < 0$):

$$f^{\text{mc}} = \frac{1}{\varepsilon_{22-}^{\text{init}}}\left[\left(\frac{\varepsilon_{22-}^{\text{init}}}{2\varepsilon_{12}^{\text{init}}}\right)^2 - 1\right](\varepsilon_{22} + \varepsilon_{33}) + \frac{1}{\varepsilon_{12}^{\text{init2}}}\left[\frac{\varepsilon_{22}^2 + \varepsilon_{33}^2}{2} + \varepsilon_{23}^2 + \varepsilon_{12}^2 + \varepsilon_{13}^2\right] \geq 1 \tag{4}$$

From the above equations, when any of the above failure variables exceed unity, damage is defined to have occurred in the composite in that specific mode. It is important to note that this failure criterion includes all components of the strain tensor. The two-dimensional failure methodology employed by ABAQUS can be obtained from Eqs. (1–4) by assuming a state of plane stress, which eliminates the out-of-plane shearing strains (ε_{13} and ε_{23}) and yields an explicit form for the out-of-plane normal strain (ε_{33}):

$$\varepsilon_{33} = \frac{1}{E_{22}}(\sigma_{33} - \nu_{23}\sigma_{22}) - \frac{\nu_{12}}{E_{11}}\sigma_{11} \tag{5}$$

In the above form, the composite is assumed to be transversely isotropic, with the plane formed by the two–three axes representing the plane of isotropy. Because of the anisotropic nature of the material, all calculations performed by the VUMAT are with respect to the local coordinate system. This provides a consistent general framework for any offaxis laminate whose local principal material directions are not aligned with those of the global system (X, Y, and Z directions in Fig. 3). Once failure has occurred in any given mode, the material response is evaluated using the damage-mechanics approach proposed by Matzenmiller et al. [15]. It is assumed that damage to the laminate in any of the four failure modes reduces the effective load-bearing area of the composite. Since a physical reduction of area is not practical in a finite element simulation, the damage-mechanics area reduction is accomplished via modification of the material's elastic constants using an internal-damage-state variable w^i. As a consequence, damage in the material at a given point reduces the tensor stress components, typical of a strain-softening constitutive model. Once any Hashin failure variable [Eqs. (1–4)] exceeds a value of 1, the internal-damage state of the material follows a rate-based progression model, similar to that proposed by Iannucci et al. [16]. The rate of propagation of damage in the material in all four modes at the current time step ($\dot{w}^i(t + \Delta t)$) depends upon the damage-state

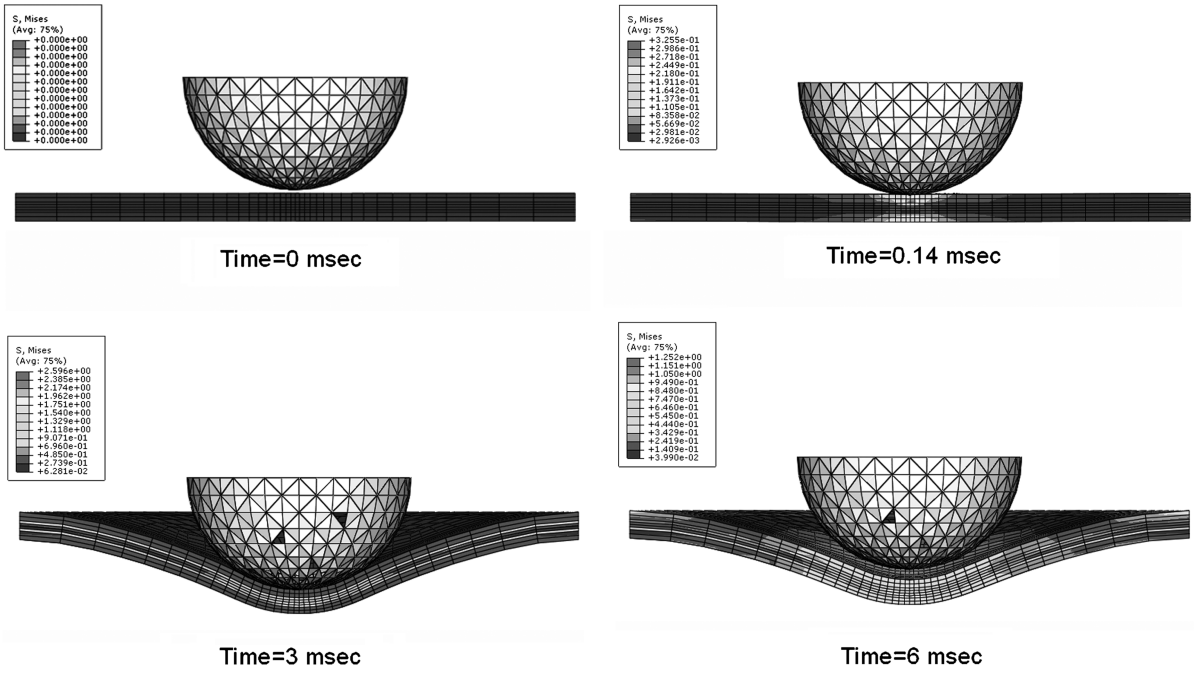

Fig. 6 Impact procedure for GLARE 5-2/1.

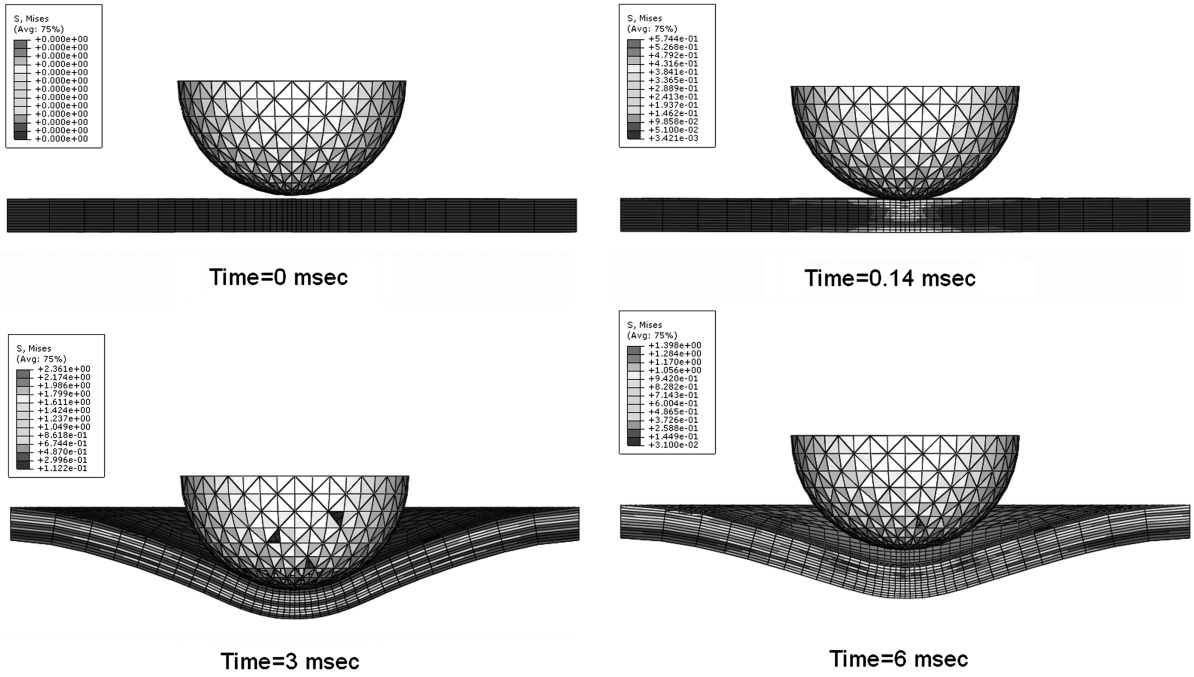

Fig. 7 Impact procedure for GLARE 4-3/2.

variable in the previous time step ($w^i(t)$) and the current strain state ($\varepsilon_{ij}(t+\Delta t)$), as well as constant damage rate terms due to crack nucleation and growth (Ω_0 and Ω_1, respectively). The explicit form for the damage propagation rate is provided in Eq. (6), in which the superscript i corresponds to each unique Hashin failure mode in Eqs. (1–4):

$$\dot{w}^i(t+\Delta t) = \Omega_0 + \Omega_1 w^i(t)\left[\left(\frac{\varepsilon_{kl}(t+\Delta t)\varepsilon_{kl}(t+\Delta t)}{\varepsilon_{mn}^{\text{init}}\varepsilon_{nm}^{\text{init}}(1-w^i(t))^2}\right)-1\right] \quad (6)$$

In the above equation, it is important to note that the strain state at failure ($\varepsilon_{ij}^{\text{init}}$) is modified by the previous damage state ($w^i(t)$). This

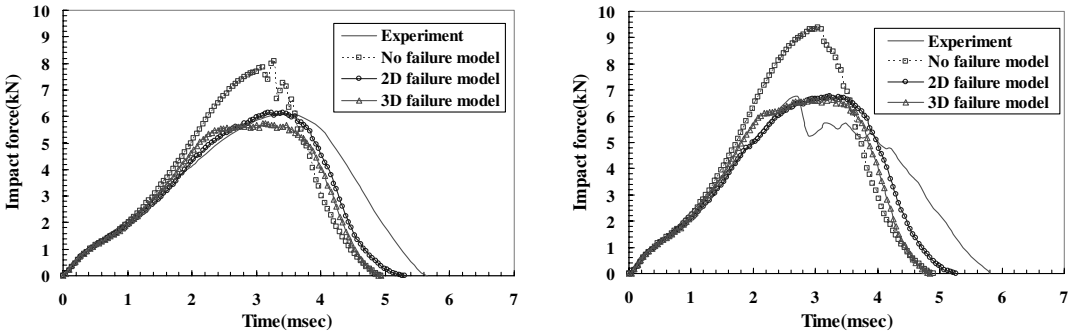

Fig. 8 Impact force–time history: comparison of experimental and simulation result for GLARE 5-2/1 with impact energy of a) 12.7 J and b) 16.3 J.

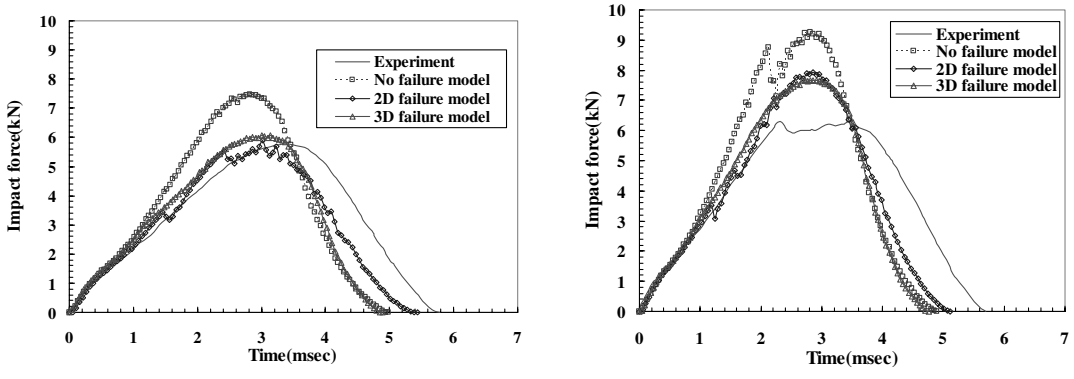

Fig. 9 Impact force–time history: Comparison of experimental and simulation result for GLARE 4-3/2 with impact energy of a) 11.4 J and b) 16.8 J.

ensures that the threshold strain value required for composite damage decreases with increasing damage density. In other words, following the initial onset of damage, the energy required for crack formation is inversely proportional to the number of cracks in the material at a given time. Since the time step between successive increments is very small (on the order of picoseconds for impact duration of 10 μs), the degradation rate of Eq. (6) is assumed to have a linear form. Thus, the damage-state variable at the current time step ($w^i(t + \Delta t)$) can be obtained from the previous damage state and the damage growth rate:

$$w^i(t + \Delta t) = w^i(t) + \dot{w}^i(t + \Delta t)\Delta t \qquad w^i \in [0, 1) \tag{7}$$

In this case, the damage-state variables must be bounded by an upper limit less than one to prevent computational issues arising during inversion when they are used to degrade the composite elastic constants according to Table 3. From the table, damage in a fiber-related mode (f^{ft}, f^{fc}) results in a decrease in the modulus in the local fiber direction (E_{11}) along with in-plane shear modulus and Poisson's ratio (G_{12} and ν_{12}, respectively). Conversely, damage in a matrix-specific mode (f^{mt}, f^{mc}) produces degradation of all elastic constants except for the modulus in the local fiber direction. Switching from a tensorial representation to a reduced index matrix form, the composite material compliance $S(t)$ at any time step can be found from Eqs. (8) and (9), in which the linear elastic material response for undamaged laminate is obtained by setting all damage-state variables to zero:

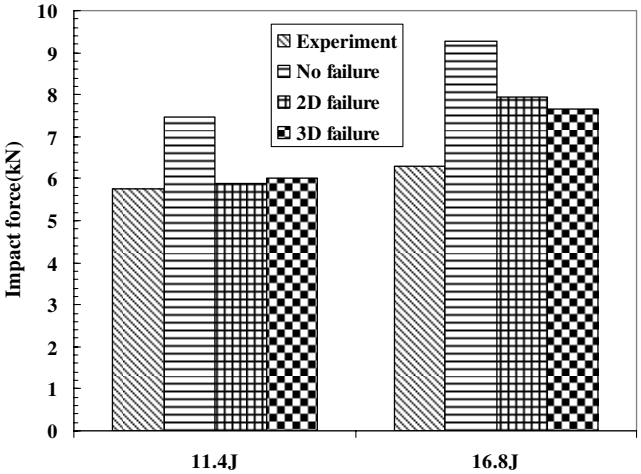

Fig. 11 Difference between predicted and measured peak impact force of GLARE 4-3/2.

the material compliance is established at the current time step, the current stress state in reduced index form can be determined from Eqs. (6–10) through inversion. For nonzero damage-state variables, it is evident that the stresses carried by a damaged element will be

$$\boldsymbol{S}(t) = \begin{bmatrix} 1/d_1E_{11} & -1/d_3(\nu_{12}/E_{11}) & -1/d_3(\nu_{12}/E_{11}) & 0 & 0 & 0 \\ -1/d_3(\nu_{12}/E_{11}) & 1/d_2E_{22} & -1/d_2(\nu_{23}/E_{22}) & 0 & 0 & 0 \\ -1/d_3(\nu_{12}/E_{11}) & -1/d_2(\nu_{23}/E_{22}) & 1/d_2E_{22} & 0 & 0 & 0 \\ 0 & 0 & 0 & 1/d_3G_{12} & 0 & 0 \\ 0 & 0 & 0 & 0 & 1/d_3G_{12} & 0 \\ 0 & 0 & 0 & 0 & 0 & 2(1 + d_2\nu_{23})/d_2E_{22} \end{bmatrix} \tag{8}$$

$$d_1 = (1 - w_{\mathrm{ft}})(1 - w_{\mathrm{fc}}) \qquad d_2 = (1 - w_{\mathrm{mt}})(1 - w_{\mathrm{mc}})$$
$$d_3 = (1 - w_{\mathrm{ft}})(1 - w_{\mathrm{fc}})(1 - w_{\mathrm{mt}})(1 - w_{\mathrm{mc}}) \tag{9}$$

$$\vec{\sigma}(t + \Delta t) = \boldsymbol{C}(\boldsymbol{t} + \Delta \boldsymbol{t})\vec{\varepsilon}(t + \Delta t)$$
$$\boldsymbol{C}(\boldsymbol{t} + \Delta \boldsymbol{t}) = \boldsymbol{S}^{-1}(\boldsymbol{t} + \Delta \boldsymbol{t}) \tag{10}$$

Note that in the above constitutive model, the transversely isotropic nature of the material is retained following the onset of damage. Once

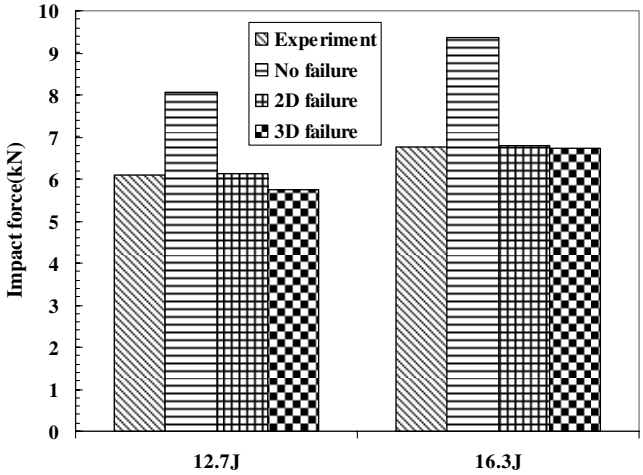

Fig. 10 Difference between predicted and measured peak impact force of GLARE 5-2/1.

smaller than those of the corresponding undamaged element, as required by the damage-mechanics assumption.

3. Energy Dissipation Due to Damage

As a consequence of the progressive failure methodology covered in the previous section, once the stiffness and compliance matrices are degraded, the material cannot revert to the undamaged state. Thus, energy is dissipated by the material due to damage formation and growth. The amount of this dissipated energy is an important quantity in impact simulations, since it represents the ability of the material to absorb the kinetic energy of the theoretically rigid

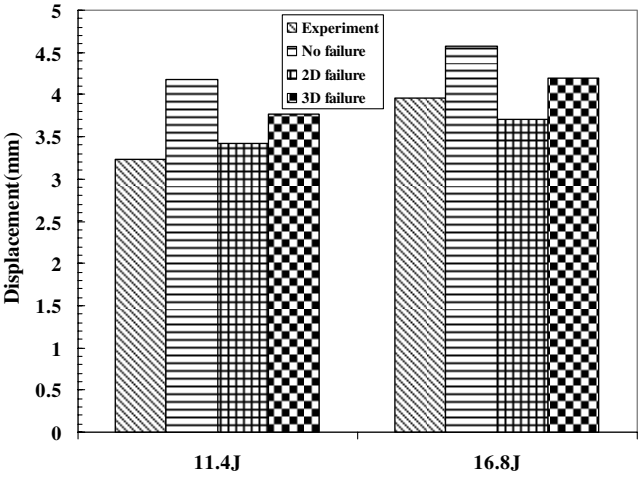

Fig. 12 Difference between predicted and measured central displacement of GLARE 5-2/1.

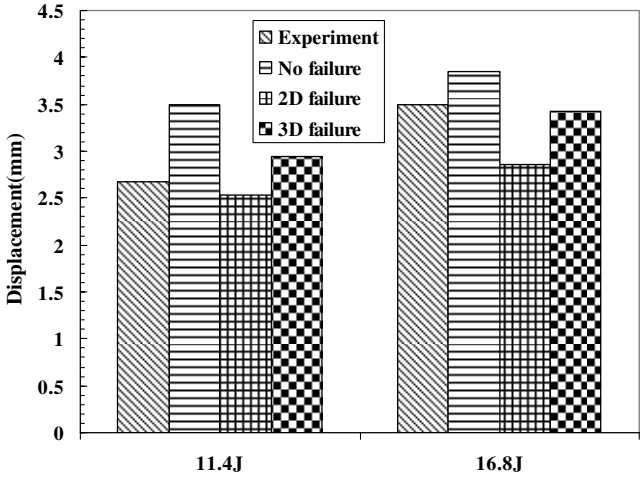

Fig. 13 Difference between predicted and measured central displacement of GLARE 4-3/2.

impactor. If thermal effects on the material are neglected, the global balance of energy for a body schematically illustrated in Fig. 5 can be established from the specified body forces, tractions, and the changes in kinetic and internal energy:

$$\int_{\partial\Gamma} v_i T_i \,\mathrm{d}S + \int_{\Gamma} v_i F_i \,\mathrm{d}V = \frac{\partial}{\partial t}\left[\int_{\Gamma}\left(\frac{1}{2}\rho v_i v_i + \rho U\right)\mathrm{d}V\right] \tag{11}$$

Applying the divergence theorem to the surface integral in the above equation and assuming that the body in Fig. 5 is at an equilibrium state, the time-integrated internal energy W can be expressed as

$$W = \int_{\Gamma} \rho U \,\mathrm{d}V = \int_0^t \int_{\Gamma} \sigma_{ij}\dot{\varepsilon}_{ij} \,\mathrm{d}V \tag{12}$$

The energy dissipated by the body due to damage formation can be determined from Eq. (12) by examining the response of the body to a constant strain field ε^*. Considering two material states, one damaged and the other undamaged (denoted by D and UD, respectively), it is evident that the stress required to deform the material by ε^* will not be the same in both cases, due to the strain-softening nature of the constitutive model. The energy dissipated by the body is equal to the difference in internal energy between the two states:

$$\Delta W = W_{\mathrm{UD}} - W_D = \int_0^t \int_{\Gamma} \sigma_{ij}^{\mathrm{UD}} \dot{\varepsilon}_{ij}^* \,\mathrm{d}V - \int_0^t \int_{\Gamma} \sigma_{ij}^{D} \dot{\varepsilon}_{ij}^* \,\mathrm{d}V \tag{13}$$

Since the strain is required to be identical in both cases, an expression linking the damaged and undamaged stress states can be determined from the constitutive relations:

$$\varepsilon_{ij}^* = S_{ijkl}^D \sigma_{kl}^D = S_{ijkl}^{\mathrm{UD}} \sigma_{kl}^{\mathrm{UD}} \qquad \therefore \sigma_{kl}^{\mathrm{UD}} = C_{ijkl}^{\mathrm{UD}} S_{ijmn}^D \sigma_{mn}^D \tag{14}$$

Inserting the above expression into the internal energy integral equation produces the following result for the dissipated energy, where I_{klmn} represents the fourth-order identity tensor:

$$\Delta W = \int_0^t \left[\int_{\Gamma} (\{C_{ijkl}^{\mathrm{UD}} S_{ijmn}^D - I_{klmn}\}\sigma_{mn}^D)\dot{\varepsilon}_{kl} \,\mathrm{d}V\right] \tag{15}$$

In the practical implementation of the progressive-damage procedure into the finite element model, this integral is evaluated in a piecewise fashion, due to the extremely small time interval between successive steps.

III. Results and Discussion

A. Comparison of Measured and Predicted Force–Time Histories

Figures 6 and 7 show the numerical impact procedure for GLARE 5-2/1 and GLARE 4-3/2. As shown in the figures, GLARE laminates

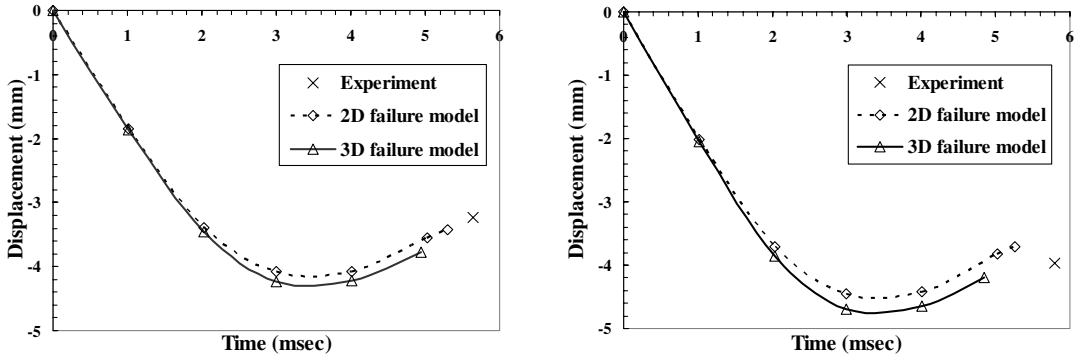

Fig. 14 Central displacement of experiment and finite element simulation with failure criteria: GLARE 5-2/1 with impact energy of a) 12.7 J and b) 16.3 J.

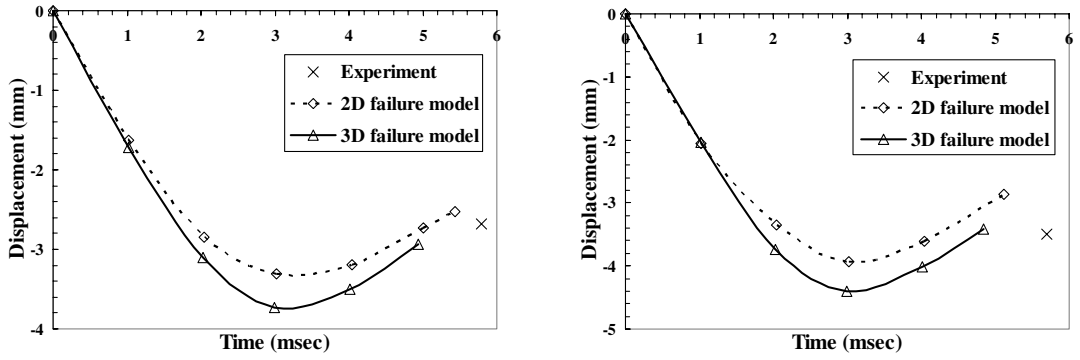

Fig. 15 Central displacement of experiment and finite element simulation with failure criteria: GLARE 4-3/2 with impact energy of a) 11.4 J and b) 16.8 J.

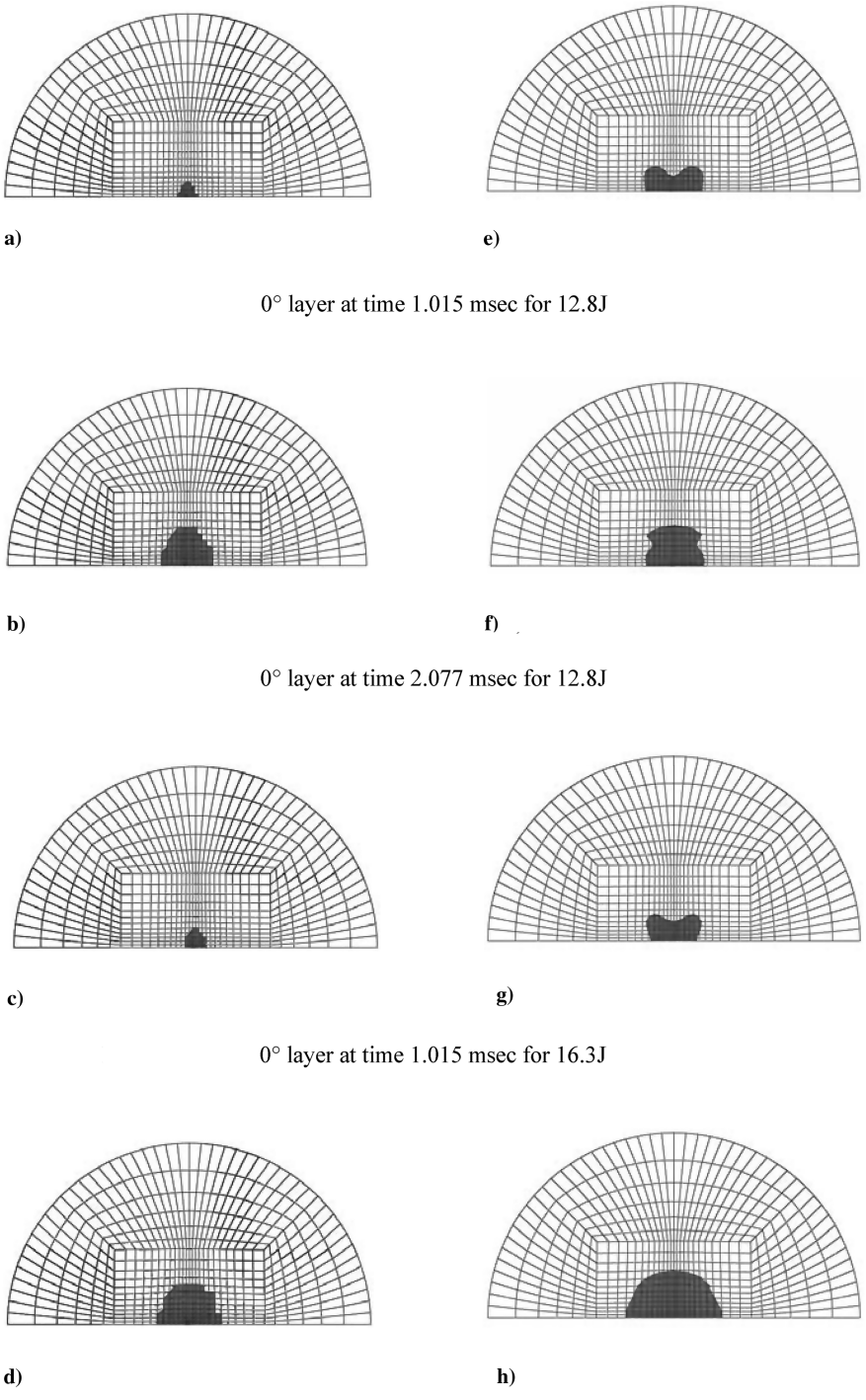

Fig. 16 Fiber tension failure-mode comparison of two-dimensional (left) and three-dimensional (right) models of GLARE 5-2/1.

experienced large deformation as a consequence of impact loading. Figures 8 and 9 show the typical peak impact force and force–time histories for GLARE 5-2/1 and GLARE 4-3/2, respectively. Additionally, the numerical simulation results are plotted for comparison with three distinct composite constitutive models: no failure criteria, two-dimensional failure criteria, and three-dimensional failure criteria. For BVID, there is no apparent impact damage apart from permanent plastic deformation in the outer aluminum layers. CVID is characterized by a sharp load drop on the force–time diagram, indicative of crack formation in the outer aluminum layer of the nonimpacted side [1]. The discrete load drops in the force–time curve after cracking, indicating delamination and failure of the composite layers [1]. For BVID shown in Figs. 8a and 9a, there is good agreement between the experimental and finite element simulation results. For low impact-energy values, it is clear that both the two- and three-dimensional failure models are capable of predicting the impact response of the material. At these impact energies, there is no significant difference between the two- and three-dimensional failure models. Both represent an improvement over a model that does not incorporate failure, as shown from the overpredictions of Figs. 8a and 9a for impact simulation without composite-failure criteria. Thus, the BVID impact energy corresponds to a limiting case in which planar failure mechanisms dominate. Figures 8b and 9b show the correlation between experiment and numerical simulation force–time histories for CVID impact energies. At these increased impact energies, it is evident that the correlation is still good. As expected, the two- and three-dimensional failure models show better predictive accuracy compared with the model

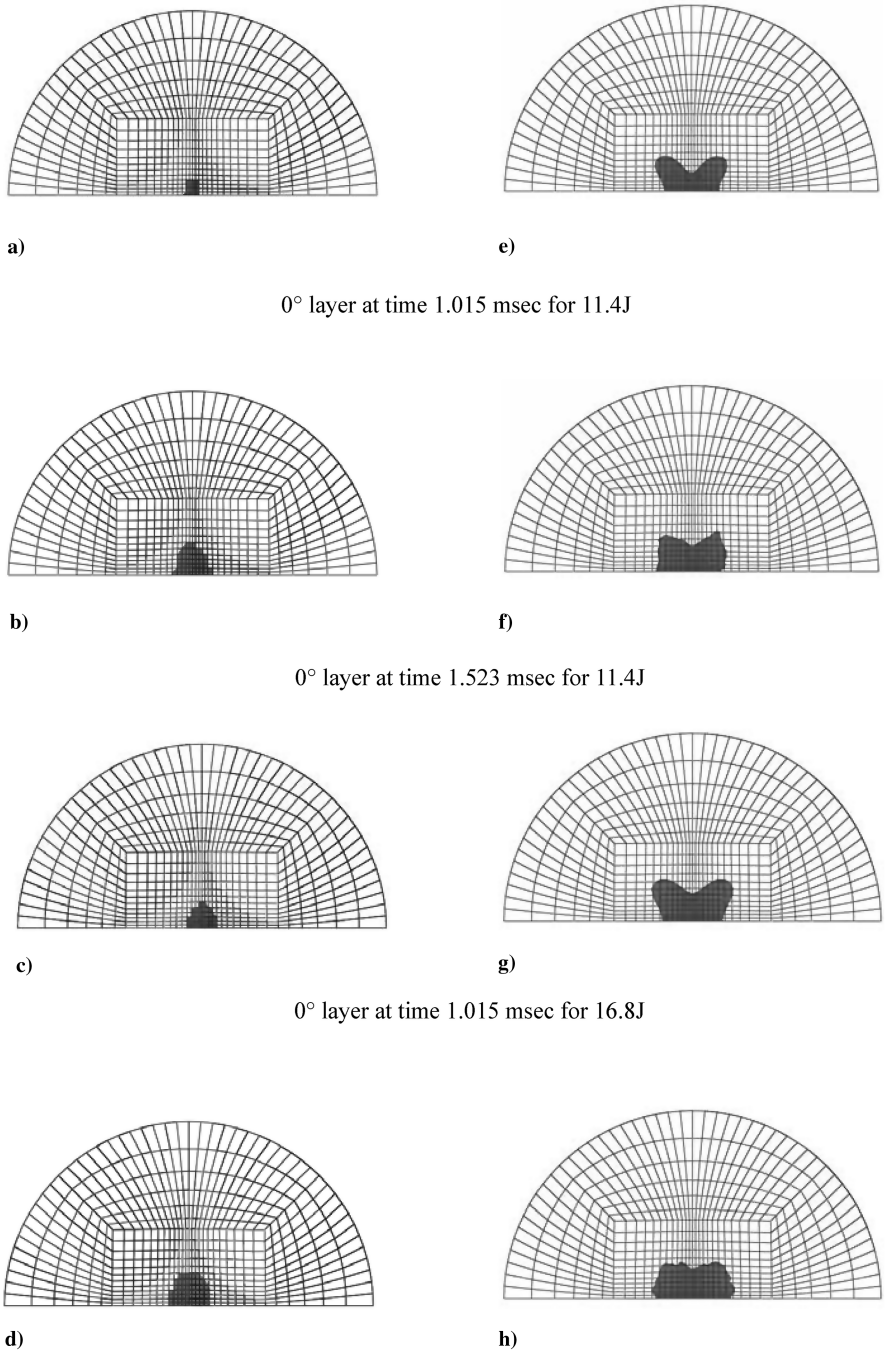

Fig. 17 Fiber tension failure-mode comparison of two-dimensional (left) and three-dimensional (right) models of GLARE 4-3/2.

that did not consider composite failure. At the energy levels required to produce CVID, composite-failure mechanisms begin to degrade the stiffness of individual laminate. As mentioned in the previous section, to model the composite degradation, a continuum damage-mechanics model was used to reduce the appropriate individual laminate stiffness component when any of the Hashin failure-initiation variables [13] exceeded a value of 1. The results of Figs. 8 and 9 show that use of the Hashin failure-criteria model as a basis for stiffness degradation of fiber-reinforced composites can improve the prediction of peak impact force and damage progression. However, despite the incorporation of composite-damage mechanisms, at high impact-energy levels, the numerical results did not show the sharp load drop that is characteristic of CVID. This discrepancy may be the result of delamination between the composite and metal layers at the nonimpacted side or cracking of the nonimpacted metal surface, with the latter phenomena being the most likely cause, since metal cracking is not explicitly included in the finite element model. Overall, however, the finite element model results display reasonable predictive accuracy. The differences between the measured and predicted peak impact force values are shown in Figs. 10 and 11. For each case, there is only a moderate difference between the two- and three-dimensional failure models in regard to predicting peak impact force. The underestimation of the impact duration in each finite element simulation can be attributed to the boundary conditions imposed by the perfect-clamping assumption and the one-dimensional displacement constraint on the rigid impactor [14].

B. Comparison of Measured and Predicted Permanent Displacement

Figures 12 and 13 show the difference between predicted and measured permanent displacement for GLARE 5-2/1 and GLARE 4-3/2 laminates, respectively. In each case, the three-dimensional

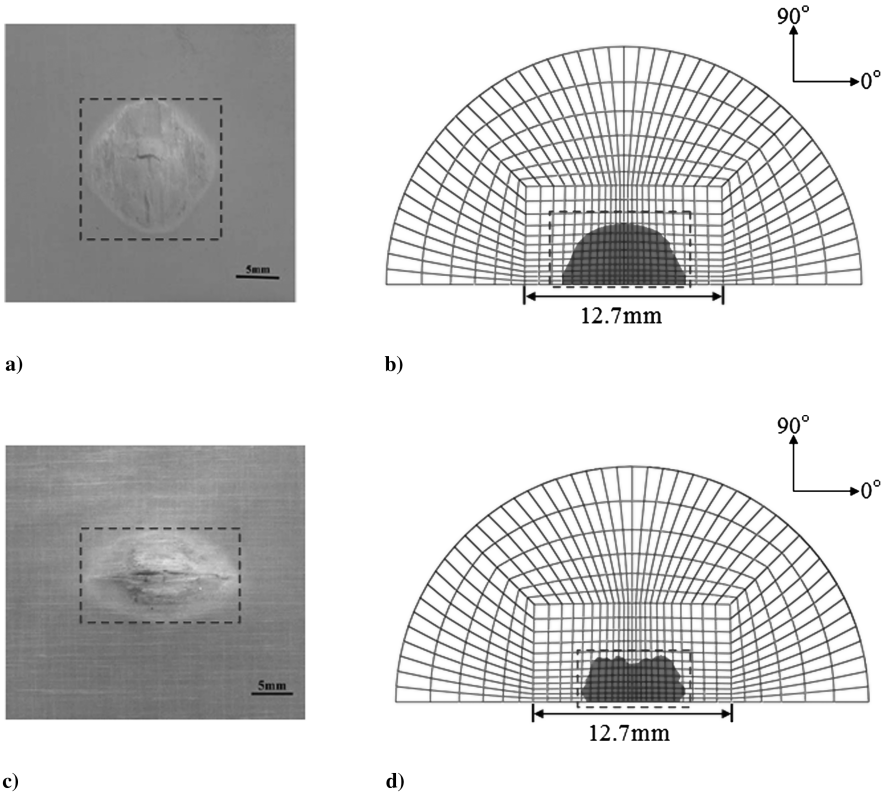

Fig. 18 Images of impact damage zone after removal of outer aluminum layers a) measured damage zone for GLARE 5-2/1 [1], b) predicted damage zone for GLARE 5-2/1, c) measured damage zone for GLARE 4-3/2 [1], and d) predicted damage zone for GLARE 4-3/2.

failure model is more compliant than the experimental results and the two-dimensional failure model. As shown in Figs. 12 and 13, for the permanent displacement, the numerical result is overpredicted, compared with the experimental result. Additionally, Figs. 14 and 15 show the change in the laminate centerline displacement as a function of the impact time. In the figures, the central displacements for the two- and three-dimensional failure models are only slightly different. The same stiffness difference between the two models shown in Figs. 12 and 13 is also evident in Figs. 14 and 15, in which the three-dimensional model predicts a much more compliant impact response at each energy level. The main cause of these discrepancies for GLARE 4-3/2 is believed to be the greater number of layers and the associated metal–composite interfaces. However, there is not a significant difference overall between the two- and three-dimensional models in terms of the permanent displacement, with both showing reasonable correlation with the experimental results.

C. Two- and Three-Dimensional Failure-Model Comparison

As mentioned in previous sections, since the thickness of composite layers is negligibly small compared with the planar dimensions, a state of plane stress can typically be assumed for the composite material, greatly simplifying the resulting failure criteria. However, under dynamic impact loading, through-thickness stress tensors σ_{13}, σ_{23}, and σ_{33} and strain tensor components ε_{13}, ε_{23}, and ε_{33} cannot be ignored, due to the three-dimensional nature of the applied loads and boundary conditions. Even though a two-dimensional failure model using continuum shell elements may produce reasonable results, a three-dimensional failure model including all stress and strain tensor components is believed to make up for the weak points of an impact simulation. Hundley et al. [17] studied the numerical simulation of the bearing strength of hybrid titanium composite laminates and showed appreciable differences between two- and three-dimensional failure models for carbon-fiber-reinforced polyimide composite materials. In this study, the damage predicted by a two-dimensional failure model was underestimated in comparison with a three-dimensional failure model. In their results, the damage of two-dimensional failure was underestimated compared with three-dimensional failure. Figures 16 and 17 show the FML Hashin failure result f_i in the 0° composite layer of GLARE 5-2/1 and GLARE 4-3/2. Figures 16a–16d and 17a–17d show the failure-criteria initiation value of the two-dimensional failure model built into ABAQUS, and the failure-criteria initiation value shown in Figs. 16e–16h and 17e–17h is simulated by three-dimensional failure model. The shaded damage area denotes the fiber tension failure initiation in the 0° composite layer. For both GLARE 5-2/1 and GLARE 4-3/2, the predicted damage shape in the three-dimensional model is significantly larger than that of the two-dimensional model. When the damage area is simulated under same impact time and energy values, the initiation of composite failure in the three-dimensional model occurs earlier than with the two-dimensional model. Figures 18a–18d show the experimentally measured damage zone in the composite layers, observed by removing the outer aluminum layer on the nonimpacted side. The damage zone for GLARE 5-2/1 in Fig. 18a is roughly circular in shape, whereas the damage zone for GLARE 4-3/2 in Fig. 18c is approximately elliptical [1]. For each GLARE variant, the damage zone in the composite layers occurred along the predominant fiber axis, i.e., equal damage growth in the 0 and 90° directions for the [0°/90°/90°/0°] layers of GLARE 5-2/1 and preferential damage growth along the 0° axis for the [0°/90°/0°] layers of GLARE 4-3/2. When the predicted damage zones of the finite element simulations are compared with the measured damage zone of experiment, it is clear that the shape of the damage envelope is similar in each case, as shown in Figs. 18b and 18d. However, at this juncture, it is important to note that the damage areas of Fig. 18 were not measured identically for the experimental and numerical cases. Experimental damage area was quantified using visually observed fiber failure resulting from out-of-plane laminated deformation, as shown in Figs. 18a and 18c. Conversely, the numerically measured damage area was determined by querying the finite element integration points at which the Hashin failure-initiation variables for fiber tension failure shown in Eq. (1) exceeded a value of 1 (Figs. 18b and 18d). Therefore, the fibers at the outer edges of the experimental damage area have only slight out-of-plane deformation as a consequence of the permanent plastic deformation in the

adjacent aluminum layers. These fibers have not fractured and are consequently not included in the finite element measured damage area. This difference in measurement technique explains why the damage envelope shape is the same for the experiments and simulations, while the actual calculated area is slightly different in each case.

IV. Conclusions

For two different kinds of impact damage (BVID and CVID), the finite element simulations were performed for single-site impact of two GLARE variants: GLARE 5-2/1 and GLARE 4-3/2. The simulation results exhibited good correlation with experimental impact tests in terms of measured force–time histories and the predicted composite-damage envelope. The only significant difference between the experimental and numerical results was that the predicted contact duration was slightly shorter in the case of the numerical simulations. This discrepancy can be attributed to the applied edge boundary conditions, which prevent vibration of the clamped area during impact. In reality, there is a small amount of clearance between the test fixture and the laminate that allows vibratory interference of the stress waves at the impacted site, prolonging the impact duration.

Additionally, this study contrasted the predicted impact response of GLARE laminates for which composite layers were modeled using two- and three-dimensional failure models. Both failure models showed good agreement with experimental results for BVID and CVID. However, the three-dimensional failure model showed more reasonable results in terms of peak impact force and permanent displacement compared with the two-dimensional failure model. In each case, for all impact energies and GLARE variants, observation of the force–time histories showed that the experimentally obtained impact resistance was slightly more compliant than predicted. Elasticity of the impactor and imperfect contact between the two bodies were not modeled and serve as possible explanations for this minor stiffness discrepancy. Visualization of the damage zone in the three-dimensional failure model via a Hashin failure-initiation-variable method resulted in excellent correlation in terms of predicted damage envelope shape.

Acknowledgments

This work was supported by the Federal Aviation Administration (FAA) under DOT/FAA 04-C-AM-UCLA-01 through the Joint Advanced Materials and Structures Center of Excellence at Wichita State University. Curt Davies is the FAA Program Manager.

References

[1] Wu, G., "The Impact Properties and Damage Tolerance and of Bidirectionally Reinforced Fiber Metal Laminates," *Journal of Material Science and Technology (Sofia)*, Vol. 42, No. 3, 2005, pp. 948–957.

[2] Vlot, A., *Glare—History of the Development of a New Aircraft Material*, Kluwer, Dordrecht, The Netherlands, 2001.

[3] Krishnakumar, S., "Fiber Metal Laminates—The Synthesis of Metals and Composites," *Materials and Manufacturing Processes*, Vol. 9, No. 2, 1994, pp. 295–354. doi:10.1080/10426919408934905

[4] Laliberte, J., and Poon, C., "Numerical Modeling of Low Velocity Impact Damage in Fibre Metal Laminates," *ICAS Congress*, International Council of the Aeronautical Sciences Paper 2002-R34, 2002.

[5] Li, C. F., Hu, N., Yin, Y. J., Sekine, H., and Fukunaga, H., "Low-Velocity Impact-Induced Damage of Continuous Fiber-Reinforced Composite Laminates. Part 1. A FEM Numerical Model," *Composites, Part A: Applied Science and Manufacturing*, Vol. 33, No. 8, 2002, pp. 1055–1062.

[6] Davies, G. A. O., Zhang, X., Zhou, G., and Watson, S., "Numerical Modeling of Impact Damage," *Composites*, Vol. 25, No. 5, 1994, pp. 342–350. doi:10.1016/S0010-4361(94)80004-9

[7] Zhang, X., "Impact Damage in Composite Aircraft Structures-Experimental Testing and Numerical Simulation," *Proceedings of the Institution of Mechanical Engineers, Part G (Journal of Aerospace Engineering)*, Vol. 212, No. 4, 1998, pp. 245–259. doi:10.1243/0954410981532414

[8] Van Rooijen, R. G. J., Sinke, J., DeVries, T. J., and Van Der Zwaag, S., "Bearing Strength of Fiber Metal Laminates," *Journal of Composite Materials*, Vol. 40, No. 1, 2005, pp. 5–19. doi:10.1177/0021998305053509

[9] ABAQUS, Software Package, Ver. 6.7, Dassault Systems Inc., Providence, RI, 2008.

[10] DeVries, T. J., "Blunt and Sharp Notch Behavior of GLARE Laminate," Ph.D. Dissertation, Delft Univ. Press, Delft, The Netherlands, 2001.

[11] Hengenbeek, M., Van Hengel, C., Bosker, O. J., and Vermeerne, C. A. J. R., "Static Properties of Fibre Metal Laminates," *Applied Composite Materials*, Vol. 10, Nos. 4–5, 2003, pp. 207–222. doi:10.1023/A:1025569316827

[12] Linde, P., Pleitner, J., De Boer, H., and Carmone, C., "Modeling and Simulation of Fiber Metal Laminates," *ABAQUS User's Conference*, 2004, pp. 421–439.

[13] Hashin, Z., "Failure Criteria for Unidirectional Fiber Composites," *Journal of Applied Mechanics*, Vol. 47, No. 2, 1980, pp. 329–335. doi:10.1115/1.3153664

[14] Nguyen, M. Q., Elder, D. J., Bayandor, J., Thomson, R. S., and Scott, M. L., "A Review of Explicit Finite Element Software for Composite Impact Analysis," *Journal of Composite Materials*, Vol. 39, No. 4, 2005, pp. 375–386. doi:10.1177/0021998305046739

[15] Matzenmiller, A., Lubliner, J., and Taylor, R. L., "A Constitutive Model for Anisotropic Damage in Fiber Composites," *Mechanics of Materials*, Vol. 20, No. 2, 1995, pp. 125–152. doi:10.1016/0167-6636(94)00053-0

[16] Iannucci, L., Dechaene, R., Willows, M., and Degrieck, J., "A Failure Model for the Analysis of thin Woven Glass Composite Structures Under Impact Loadings," *Computers and Structures*, Vol. 79, No. 8, 2001, pp. 785–799. doi:10.1016/S0045-7949(00)00190-5

[17] Hundley, J. M., Yang, J.-M., Hahn, H. T., and Facciano, A. B., "Bearing Strength Analysis of Hybrid Titanium Composites Laminates," *AIAA Journal*, Vol. 46, No. 8, 2008, pp. 2074–2085. doi:10.2514/1.36242

A. Pelegri
Associate Editor